Accelerated reliability testing of highly aligned single-walled carbon nanotube networks subjected to DC electrical stressing

2011 Nanotechnology 22 265713

(http://iopscience.iop.org/0957-4484/22/26/265713)

Nanotechnology **22** (2011) 265713 (9pp) doi:10.1088/0957-4484/22/26/265713

Accelerated reliability testing of highly aligned single-walled carbon nanotube networks subjected to DC electrical stressing*

Mark C Strus[1,4], Ann N Chiaramonti[1], Young Lae Kim[2], Yung Joon Jung[3] and Robert R Keller[1]

[1] Materials Reliability Division, National Institute of Standards and Technology, Boulder, CO 80305, USA
[2] Electrical and Computer Engineering, Northeastern University, Boston, MA 02115, USA
[3] Mechanical and Industrial Engineering, Northeastern University, Boston, MA 02115, USA

E-mail: mark.strus@nist.gov

Received 20 December 2010, in final form 7 April 2011
Published 18 May 2011
Online at stacks.iop.org/Nano/22/265713

Abstract
We investigate the electrical reliability of nanoscale lines of highly aligned, networked, metallic/semiconducting single-walled carbon nanotubes (SWCNTs) fabricated through a template-based fluidic assembly process. We find that these SWCNT networks can withstand DC current densities larger than 10 MA cm^{-2} for several hours and, in some cases, several days. We develop test methods that show that the degradation rate, failure predictability and total device lifetime can be linked to the initial resistance. Scanning electron and transmission electron microscopy suggest that fabrication variability plays a critical role in the rate of degradation, and we offer an empirical method of quickly determining the long-term performance of a network. We find that well-fabricated lines subject to constant electrical stress show a linear accumulation of damage reminiscent of electromigration in metallic interconnects, and we explore the underlying physical mechanisms that could cause such behavior.

S Online supplementary data available from stacks.iop.org/Nano/22/265713/mmedia

(Some figures in this article are in colour only in the electronic version)

1. Introduction

Due to their high current-carrying capability [1] and appreciable thermal conductivity [2, 3], single-walled carbon nanotubes (SWCNTs) have emerged as an ideal material for future nanoscale electronics [4, 5]. The unique quasi-one-dimensional shape [6] and strong sp^2-and π-bonding between neighboring carbon atoms [7] in SWCNTs allows for large electron mean free paths [8, 9], meaning carbon nanotubes (CNTs) can conduct ballistically under ideal circumstances while withstanding current densities in excess of 10^9 A cm^{-2} [10]. Because of this high electrical conductivity and hypothesized resistance to electromigration [10, 11], the 2009 International Roadmap for Semiconductors (ITRS) [12] has suggested electrically contacted bundles of carbon nanotubes [13–15] could eventually replace copper as interconnect width requirements shrink below 40 nm. However, the ability to assemble highly aligned SWCNTs and connect them reliably to metal electrodes remains a significant challenge.

The electrical advantages of CNTs have also been explored through the fabrication of networked SWCNT films [16–18]. Such networks are readily fabricated at low cost and are elastically flexible at high mechanical strains [19], so they can be mounted to bendable polymers to form

* Contribution of NIST, an agency of the US government; not subject to copyright in the United States.
[4] Author to whom any correspondence should be addressed.

new classes of flexible electronics with applications such as field effect transistors [20–23] and chemical sensors [24–27]. These networks are optically transparent with sheet resistances approaching that of conventional transparent conducting oxides (TCO) such as indium tin oxide (ITO) [28], making them viable candidates to replace transparent conducting electrodes in flat-panel displays and photovoltaics [29–33].

Despite their attractive electronic properties, most of the literature has focused on either the scientific properties of individually wired CNTs [34] or how to improve fabrication techniques of CNTs in bundles, arrays and networks for specific applications [35]. Several studies have examined how CNTs can fail from resistive heating when exposed to extremely high current densities [36–38], an effect that is more pronounced in air, where oxidation plays a role [39, 40]. In each of these studies, CNTs failed in a matter of seconds when current was rapidly applied. As such, these results are not able to predict long-term electrical degradation and lifetime to open-circuit failure under more realistic operating conditions.

The long-term performance and reliability of CNT-based devices have been largely neglected, despite their likely exposure to significant current densities and high temperatures that may directly induce thermal failure [36], cause thermal–mechanical fatigue or stimulate de-adhesion and significant interdiffusion at critical interfaces between CNTs, metals, dielectrics and polymers [41, 42]. Because CNT electrical properties are known to be sensitive to growth conditions and process variability [43], tools to monitor and predict their electrical reliability are needed to improve process design and ensure that CNT-based commercial devices exhibit long lifetimes. The few published CNT reliability measurements have concentrated on running large currents in a single nanotube for long periods [10, 11]. The apparent lack of any measurable accumulation of damage over time suggests that the strong, covalently bonded carbon atoms in individually wired CNTs may not be subject to electromigration, as further supported by the observed electromigration resistance of CNT–Cu composite interconnects [44, 45]. However, all of these studies were based on single CNT failures without any repeated experiments to confirm the results and gather statistics. We are unaware of any studies investigating the long-term reliability and performance of SWCNT networks.

In this paper, we present test methods designed to investigate the electrical reliability of lines of highly aligned, networked SWCNTs. We observe two distinct types of damage accumulation with correspondingly different rates of degradation. We offer methods of determining *a priori* whether a CNT array has been properly fabricated for good long-term reliability and whether it can endure considerable current stressing for long periods. Based on these empirical data, we hypothesize the underlying physical degradation mechanisms that may be responsible for these device failures.

2. Experimental methods

Super-aligned networks of SWCNTs, such as the one shown in figure 1, were fabricated by a template-based fluidic assembly process fully described in [46, 47]. Briefly, an Si substrate

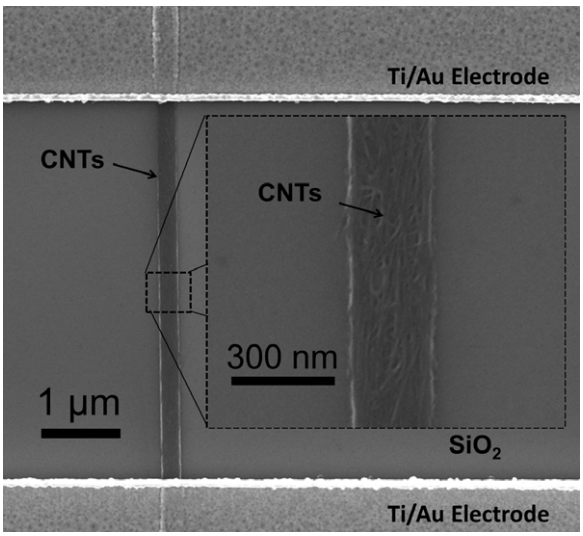

Figure 1. SEM image of highly aligned network array of SWCNTs fabricated by a template-based fluidic assembly process [71] with Ti/Au electrodes deposited by a standard EBL process. The linewidth and length were 200 nm and 5 μm, respectively, whereas the height varied because of the fabrication process (see figure 2). The typical length of individual SWCNTs was 800 nm. The inset shows a higher magnification image of a typical SWCNT array line with discernible SWCNT bundles. Both images are of lines that failed via DC electrical stressing, but the SEM images revealed no obvious morphological alterations due to failure.

with a thermally grown 100 nm SiO_2 film was plasma-treated to enhance its hydrophilic nature. Polymethyl methacrylate (PMMA) photoresist patterns constructed via electron beam lithography (EBL) were used to pattern nanoscale lines. These templated substrates were dip-coated at a constant pulling rate into a solution of deionized (DI) water without any added surfactants containing a naturally occurring population of 1/3 metallic SWCNTs (m-SWCNTS) and 2/3 semiconducting SWCNTs (s-SWCNTs). The SWCNT population had an average length of 610 nm and an average diameter of 1.1 nm, based on our Raman spectroscopic analysis. The SWCNTs adhered mainly to the underlying SiO_2 surface and self-assembled as aligned bundles. The PMMA and surfactant were then removed, and conventional EBL was used to deposit Ti/Au electrode pads (5 nm and 150 nm thick, respectively) on top of the SWCNT arrays to form the final test structure shown in figure 1.

Although the width (200 nm) and length (5 μm) of the assembled SWCNT lines were well defined by the PMMA channels, the final fabricated height depended on the thickness of the PMMA and the pulling rate. Although the intention was to deposit arrays with constant heights of 20 nm across the width of the line, cross-sectional transmission electron microscope (TEM) images (figure 2(a)) of a typical line showed height variations, with CNTs agglomerating near the edges of the PMMA channels during fabrication. Despite careful efforts to eliminate process variability, there was clear variation in the cross-sectional area among the different lines as well as along a single SWCNT line. In all lines, the SWCNTs appeared densely packed, as shown in the TEM cross-sectional

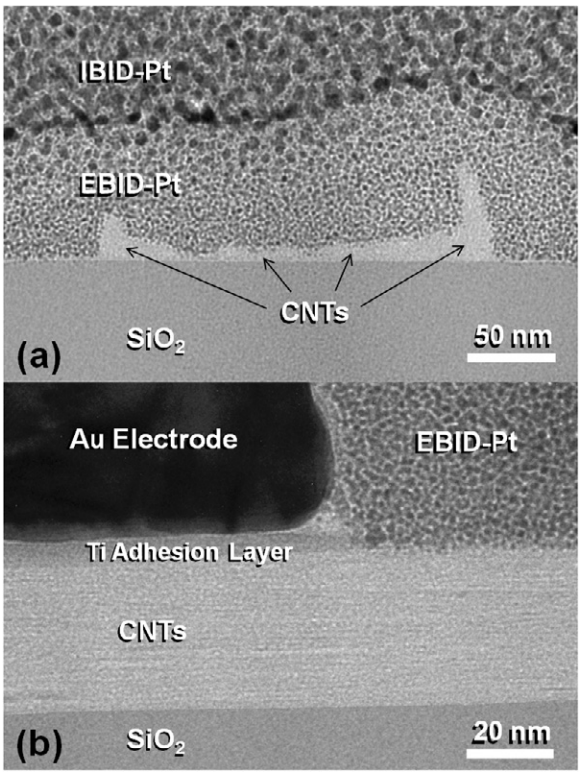

Figure 2. Orthogonal TEM cross-sectional images of two different networked SWCNT lines cut (a) perpendicular and (b) parallel to the line. Both were prepared by the focused-ion-beam (FIB) lift-out process, whereby electron-beam-and ion-beam-induced deposition of platinum (EBID-Pt and IBID-Pt, respectively) are used to protect the sample from the normally incident Ga+ ions used for thinning to electron transparency. The transverse cross section of the SEM array in (a) shows more SWCNTs near the edges at the location of the PMMA mask (previously removed here), while the longitudinal cross section in (b) shows that the CNTs are densely packed underneath the Au/Ti electrode. The SWCNTs cross-sectional area in (a) was estimated to be approximately $\approx$3000 nm^2 $\pm$ 500 nm^2. Contrast in the SiO_2 substrate has been artificially enhanced for clarity using a grayscale overlay.

image of a typical SWCNT network cut lengthwise near a Ti/Au electrode (figure 2(b)). We tested dozens of SWCNT lines on three separate wafers fabricated at different times (up to several months apart) and witnessed no trends between the electrical results and the particular wafer tested.

All measurements were obtained by the use of pseudo-four-terminal sensing in air at room temperature with a commercial power supply, where both the applied voltage source and current sensing tungsten probes were placed on the same Ti/Au electrode pairs. Thus, the measurement probe resistances were removed from the resistance measurement of the total system, but the contact resistance between the SWCNTs and Ti/Au electrode was included. Because of experimental constraints, we did not know the actual contact resistances between the metal electrodes and SWCNT lines presented here. However, typical contact resistances from several lines on the same wafers were found to be $\approx$5% of the total line resistance, except for a few outliers where the contact resistance was as high as 50%. In this work, we report only total line resistance, which includes the resistances of the CNT–electrode interface, the individual SWCNTs and the SWCNT–SWCNT junction resistances.

Although networks of SWCNTs can be made by a variety of techniques including spray coating, vacuum filtration or electrophoretic deposition, networks made from dip-coating techniques typically have the smallest surface roughness and lowest resistance [48]. Assuming ideal close-packing and a typical cross-sectional area of approximately 3000 nm^2 $\pm$ 500 nm^2 (based on figure 2), our networked SWCNT lines were found to have resistivities in the range 1.7–18 mΩ cm, consistent with recent studies of similar arrays [49, 50]. The nominal resistance of each specimen was obtained before electrical stressing from the slope of the linear I–V measurements, where the applied voltage was ramped from -1 to 1 V. At these low voltages, all lines presented here behaved ohmically.

3. Experimental results

Each networked SWCNT line was subjected to a constant DC input voltage V_{input}, which was varied from line to line, while the current (I_{measure}) was collected as a function of time. The input voltage was always ramped from 0 to V_{input} over the course of several minutes (not shown). The magnitude of V_{input} was chosen differently for each line to explore the effect of the electrical stress magnitude. If the chosen values of V_{input} were too small (typically <4 V), the lines would last several days with no signs of damage. The SWCNT array lines were placed on a heat-controlled chuck, and the resistance was found to decrease nonlinearly with an increase in temperature, as is typical of other SWCNT networks [50–52]. The current densities in the networked CNT lines were found to be between 0.93 and 9.7 MA cm^{-2}, as calculated by dividing the maximum I_{measure} in each line by the cross-sectional area of a 'typical' line, assuming full packing density (see figure 2(b)). Actual current densities in individual SWCNTs were probably higher, because it was likely that some of the SWCNTs in the cross section did not conduct equally or at all, and the SWCNT packing density must be <1.

Figure 3 shows long-term DC current stressing results for several networked SWCNT lines, where $R_{V/I}(t) = V_{\text{input}}(t)/I_{\text{measure}}(t)$ is plotted as a function of time. Because of the nonlinear I–V relationship at high voltages (>1 V), $R_{V/I}(t)$ represents the instantaneous resistance (not to be confused with differential resistance) and essentially tracks inversely to changes in current, because the voltage is always held constant. The instantaneous resistance has been normalized such that $||R_{V/I}|| = R_{V/I}(t)/R_{V/I}(0)$, where $t = 0$ was defined as the point when the voltage reached the constant V_{input} value after the initial ramp. In several of the tests (blue circles), $||R_{V/I}||$ increased (I_{measure} decreased) linearly and predictably until moments before open-circuit failure, when $||R_{V/I}||$ rose (I_{measure} declined) very suddenly. In other experiments (red triangles), $||R_{V/I}||$ increased over time but in an unpredictable manner, with time-dependent changes in the rate of degradation, sudden jumps in $||R_{V/I}||$ and, in

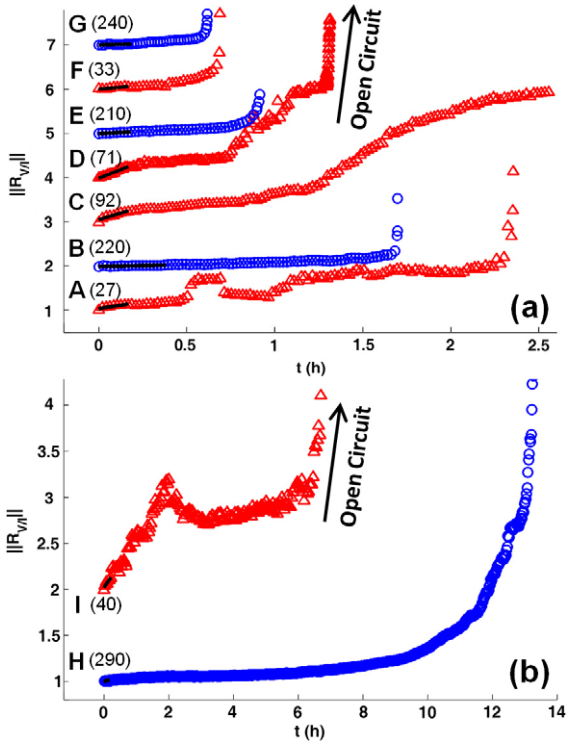

Figure 3. DC electrical stressing measurements for several networked SWCNT lines, where $||R_{V/I}||$ is the instantaneous resistance of the line as it is subjected to a constant applied voltage. $||R_{V/I}||$ data was collected every 2 s, but values at every 30 s are plotted here for clarity. Except for lines **A** and **H**, each of the lines has been offset by an integer multiple so that all tests could be plotted simultaneously. $||R_{V/I}(0)||$ always equals 1. The numerical values in parentheses indicate the starting current in each networked line (in μA) at the beginning of the DC electrical hold. Two graphs are presented because (b) shows lines with longer lifetimes. Two distinct types of degradation emerge, as distinguished by either the blue circles or red triangles. The overlayed solid black lines are the best linear fits of $||R_{V/I}||$ as described in the text, which are used to calculate the normalized rate of degradation in figure 4.

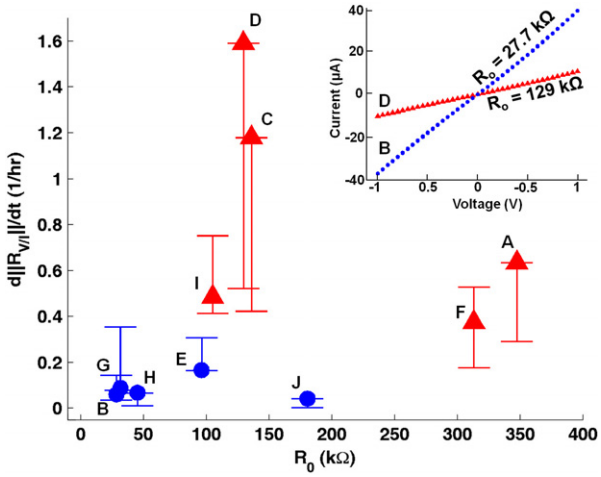

Figure 4. Normalized rate of degradation derived from figure 3 plotted as a function of initial resistance for several networked SWCNT lines. The error bars indicate the range of possible degradation rates from $t = 0$ to t_f as described in the text, while the plotted point is the slope of the best linear fit (see black lines in figure 3). The two different types of degradation are clearly separated. The inset shows typical ohmic behaviors before electrical stress measurements for two different lines (**B** and **D**), which exhibit different types of degradation.

some cases, such as in tests **A** and **I**, an unexpected decrease in $||R_{V/I}||$ (increase in I_{measure}) as a function of time.

The initial rate of degradation, $\mathrm{d}||R_{V/I}(t)||/\mathrm{d}t$, in each networked SWCNT line was calculated by fitting a line to the $||R_{V/I}||$ versus t data of figure 3 from $t = 0$ to a given t_f, as long as $t_f > 10$ min and $||R_{V/I}(t_f)|| < 1.5$. These cutoff parameters ensured that degradation rates were obtained after a sufficient amount of time to reach a steady-state temperature, but well before open-circuit failure. The best least-squares fit is shown in figure 3 and the corresponding rate $\mathrm{d}||R_{V/I}||/\mathrm{d}t\,(t)$ is plotted in figure 4 as a function of the nominal line resistance, R_o, measured before electrical stressing. The error bars in figure 4 correspond to all of the possible degradation rates from linear fits within the specified time range.

Figure 4 further highlights the two different kinds of degradation observed in figure 3, namely that (a) the networked SWCNT lines that damaged linearly and predictably (blue circles) possessed relatively low initial resistances and steady, slow degradation rates, whereas (b) lines with relatively high initial resistances (red triangles) were likely to degrade unpredictably and at a faster rate. Because R_o was primarily influenced by the fabrication process variability, figure 4 offers a quick empirical screening technique to distinguish whether changes in processing may affect long-term DC reliability.

The existence of two distinct types of degradation is reinforced by figure 5, where the degradation rate was plotted against the initial input power ($P = I_{\text{measure}} V_{\text{input}}$ at $t = 0$). Here, the unpredictable, 'poorly fabricated' SWCNT lines are shown to have had very fast degradation rates, despite the fairly low power input. On the other hand, 'well-fabricated' SWCNT lines, which behaved more predictably, degrade at similar rates despite different input powers.

In Al and Cu metallic interconnects, electromigration tests are used to define empirical relationships between current density and time to failure, typically defined as the point when line resistance increases 3%–10% from its initial value [53–55]. These tests are then used to define the maximum allowable current densities in normal operation to ensure sufficient device lifetime for the particular application. Although we cannot determine the exact current density in individual networked SWCNT lines because the cross sections of current-carrying SWCNTs are unknown, we can obtain an empirical relationship between input power and time to failure, defined here as a 5% change in $||R_{V/I}||$ from $t = 0$ (see figure 6). All of the networked SWCNT lines with erratic failure behavior (red triangles) failed within a short period (<12 min), despite the low input power. Lines exhibiting a linear decrease in current (blue circles) lasted significantly longer, some as long as several hours, before the instantaneous resistance changed appreciably, and the lifetime to failure was seemingly independent of power input to the line.

4. Discussion

The networked SWCNT lines subjected to constant DC electrical stressing in this study exhibited two distinct types

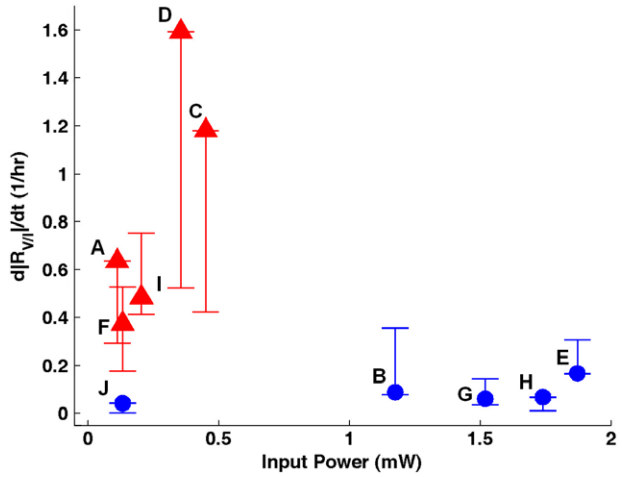

Figure 5. Different degradation behavior is evident when the rate of degradation is plotted against the input power. Networked SWCNT lines with high initial resistance (see figure 4) caused by poor fabrication (red triangles) degrade quickly even at relatively low input powers, and the degradation rate appears proportionally linked to the input power. Lines with low initial resistances (blue circles) show the same degradation rate despite different input powers, suggesting that the degradation mechanism is not strongly dependent on the amount of electrical stressing.

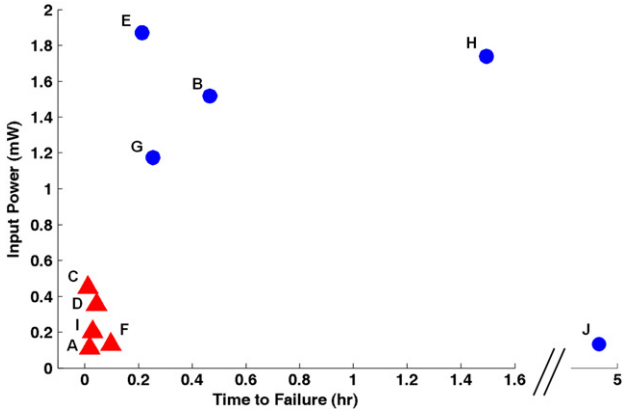

Figure 6. None of the networked SWCNT lines with unpredictable $||R_{V/I}||$ behavior (red triangles) lasted longer than 12 min, whereas the lines that exhibit progressive accumulation of damage (blue circles) exhibited much longer lifetimes despite high input powers. At low input power, line **J** lasted nearly 5 h before failing (defined as a 5% change in $||R_{V/I}||$).

of failure, as reflected in normalized instantaneous resistance lifetime data: (i) a noisy, more discretized buildup of damage, leading to an unpredictable onset of open-circuit failure (red triangles) and (ii) a smooth, gradual, linear buildup of damage, leading to a threshold above which open-circuit failure occurred (blue circles). Although conventional SEM imaging techniques have so far proven insufficient to reveal either the structural form of the damage or the location of the open circuit (see figure 1, imaged after DC induced failure), we believe these two failure mechanisms are distinguishable because of their different dependence on input power. We consider two possible mechanisms at this point: oxygen desorption and progressive breakdown of CNT–CNT conduction paths via resistive heating and oxidation. We believe that both of these mechanisms are present to some extent in the degradation of all of the lines, but that the density of initial conduction paths determines the rate and predictability of damage progression.

The discretized damage buildup in samples **A, C, D, F** and **I**, coupled with the observation of higher initial resistances, suggests that fewer conduction paths initially exist within the CNT array prior to stressing, compared to the 'good' samples (**B, E, G, H** and **J**). In the line, current flow follows the lowest resistance path through the SWCNT network, although shunting paths may also exist. When a path of low resistance breaks down, the next lowest resistance path would carry current, consistent with an overall increase in the instantaneous resistance. This type of behavior has been observed in multi-walled CNTs, where individual shells break down one by one from localized resistive heating [36–38] and oxidation [39, 40]. In a CNT network, a breakdown in a conduction path could take place over different size scales and at various locations, such as individual CNT shell oxidation, CNT–metal disintegration, bundle contiguity changes or thermal breakdown of CNT–CNT junctions.

On the other hand, the smooth, gradual buildup of damage in samples **B, E, G, H** and **J** is reminiscent of the gradual decrease in conductivity observed during electromigration void formation and growth [56–59] in uniform metal interconnect structures. This type of damage accumulation suggests that the physical defects responsible for the increase in the instantaneous resistance form and extend in all regions of the structure with similar likelihood. In other words, many conduction paths through the network are in operation at the same time from the onset of stressing, and the SWCNTs comprising these paths are subjected to similar conditions of current density, heightened temperature and mechanical stress. Because several conduction paths initially exist, the remaining paths experience only a slight increase in current load when a single conduction path breaks down.

We developed the simple model in figure 7(a) to investigate how the number of initial conduction paths, N_{paths}, might affect the overall resistance of a networked SWCNT line. The overall line resistance is plotted against the number of parallel conducting paths, which were randomly generated from a normal distribution with a mean of 100 kΩ and a standard deviation of 10 kΩ. The inset in figure 7(a) shows the normalized distribution of resistances of the conducting paths for three lines with different values of N_{paths}. Clearly, the overall line resistance decreases as more parallel conducting paths are included. This result agrees with previous studies that showed that the overall SWCNT network resistivity increased in thicker [49] and more dense [60] networks. Clearly, when a network has more nanotubes, especially if those SWCNTs are optimally oriented [61], the overall network resistivity is lower because the number of conduction paths is larger.

It follows that the overall resistance of the SWCNT network will increase whenever an individual conduction path is broken. Figure 7(b) shows how the overall line resistance decreases as conducting paths are removed for the three

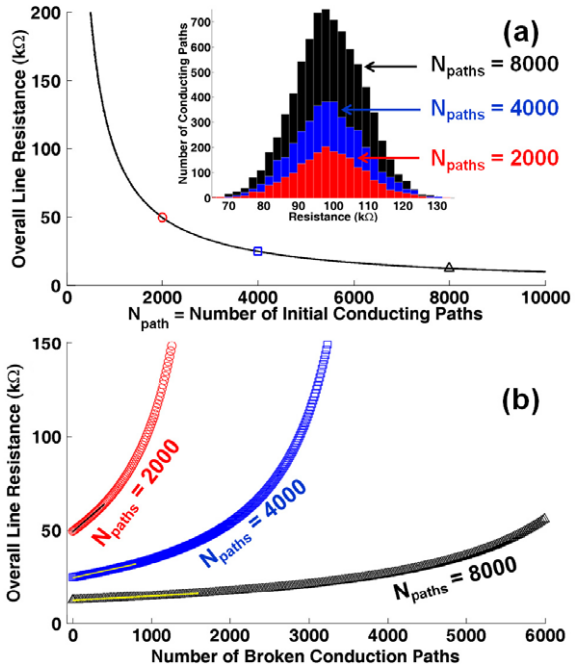

Figure 7. (a) Model demonstrating how the overall resistance in a networked SWCNT line depends on the number of initial conducting pathways, N_{paths}, assumed here to be normally distributed with a mean value of 100 kΩ and standard deviation of 10 kΩ. All the conduction paths operate together in parallel. The inset shows the distribution of resistances for three lines with different values of N_{paths}. In (b), the overall resistance of the three lines is plotted as a function of the number of conduction paths that have been broken from the initial line. In each iteration, the single conduction path with lowest resistance (highest current) is subsequently removed to simulate single-path breakdown. The overlayed linear lines show how degradation rate as defined in figure 3 could depend on the number of initial paths, although there is no time dependence included in this model.

lines in figure 7(a) with different values of N_{paths}. In each progressive step, the conduction line with the lowest resistance is removed, simulating a situation where the conduction path with the highest current breaks from high heat and/or possible oxidation. Although no time dependence is included in figure 7(b), the results are qualitatively similar to our experiment results, namely that lines with initially higher overall resistance (on account of fewer N_{paths}) degrade at a quicker rate. When very few conduction paths remain in the line, the breakdown of another path causes a large change in the overall resistance, which creates the nonlinear behavior immediately before open circuit (no more conduction paths) that was similarly observed in figure 3.

While this simple model explains the importance of the number of initial conduction paths, it cannot account for the time-dependent breakdown of individual conduction paths or explain the unpredictable damage buildup in samples **A, C, D, F** and **I**. However, the fact that the initial normalized rate of degradation ($\mathrm{d}||R_{V/I}||/\mathrm{d}t$) in these particular lines scales with the input power (see figure 5) suggests that higher temperatures accelerate the degradation and eventual breakdown. In fact, we observed clear failure in CNT bundles when increasing voltages were applied to a line within a few minutes until open-circuit failure (see supplementary information available at stacks.iop.org/Nano/22/265713/mmedia). Estrada and Pop [62] showed, through infrared thermal imaging, that such visible breaks corresponded to localized 'hot spots'. These results coupled with our power-dependent breakdown observations suggest heat dissipation may be responsible for damage accumulation and eventual network breakdown. Because localized resistive heating and oxidation are most likely to occur at the location of highest electrical resistance [63], the individual CNT–CNT junctions are a likely candidate for conduction pathway breakdown.

For the low initial resistance lines (**B, E, G, H** and **J**), the normalized rate of resistance is independent of the input power over a full order of magnitude, suggesting that there is a threshold value above which damage starts accumulating, and that the underlying mechanism is the same throughout the power range. Although breakdown of the conduction paths could be responsible for this damage accumulation, the tremendous predictability of this degradation behavior suggests that all conducting paths are affected simultaneously, a result that may be explained by dopant desorption or some other thermally dependent process.

Recent results have shown that the resistivities of SWCNT networks were sensitive to the presence and desorption of dopants [50, 51, 63]. When exposed to air, CNT absorption of O_2 molecules inadvertently caused a p-type doping effect on the network [64] and lowered the sheet resistance [51]. O_2 molecules adsorbed at SWCNT interfaces created local electrical fields that modified the shape and height of tunnel barriers and led to a higher degree of carrier delocalization [50, 65]. This improved conductivity is not limited to O_2, as adsorbed H_2O molecules, which may remain in our samples from the fluidic assembly process, have been shown to enhance the p-type doping effect of O_2 [66]. When subjected to high electrical currents [67] or high temperatures [51, 63], dopant molecules were found to desorb from the surface, which led to higher network resistances.

In our case, the high current stressing that is likely to be accompanied by resistive heating could cause desorption of initially present O_2 or H_2O and appear as the gradual accumulation of damage (increase in $||R_{V/I}||$) in figure 3. In line with fewer initial conduction paths, dopant desorption would lead to even faster initial rates of degradation, because the number of carriers that remain localized would be a larger fraction of the total carriers available [68]. This effect would put additional stress on the few remaining low resistance pathways to carry the bulk of the current, and further accelerate the discrete breakdowns observed.

5. Conclusions

Through high current density DC electrical stressing, we have investigated the reliability of networked SWCNT lines fabricated by template-guided fluidic assembly. Our electrical stress tests uncovered two distinct types of degradation. The first type occurred more randomly with high degradation rates, while the second manifested itself as a highly predictable, slow accumulation of damage. This DC electrical stress test

is a useful way to quickly screen for proper fabrication of a CNT network and its reliability for long-term performance. Although developed for a specific type of networked SWCNT lines, the experimental methods are simple and could be readily adapted for reliability testing of individual CNTs, CNT bundles and vias, or other current-carrying nanowires.

Due to the small size and buried nature of individual and bundled SWCNTs, as well as the proneness of the surrounding SiO_2 to charging, we were unable to observe the underlying failure mechanism with conventional SEM microscopy techniques. We have suggested that the degradation of the lines is due to progressive conduction path failure coupled with O_2 and H_2O desorption. However, this hypothesis requires further experimental validation. Other techniques such as post-mortem and *in situ* TEM [36], voltage contrast SEM [69] and conductance atomic force microscopy [63, 70] are currently underway to obtain further insights.

Acknowledgments

The authors thank the NIST Office of Microelectronics Programs and the National Research Council for supporting this work. The authors are grateful to A Smolyanitsky, D T Read and N Barbosa III from the NIST Materials Reliability Division in Boulder, CO for their helpful insight and review of this work, and L Robins for his Raman spectrum analysis. YJJ acknowledges the support from the NSF-ECCS program (0925566).

References

[1] Kasumov A Yu, Deblock R, Kociak M, Reulet B, Bouchiat H, Khodos I I, Gorbatov Yu B, Volkov V T, Journet C and Burghard M 1999 Supercurrents through single-walled carbon nanotubes *Science* **284** 1508–11

[2] Hone J, Whitney M, Piskoti C and Zettl A 1999 Thermal conductivity of single-walled carbon nanotubes *Phys. Rev.* B **59** R2514–6

[3] Kim P, Shi L, Majumdar A and McEuen P L 2001 Thermal transport measurements of individual multiwalled nanotubes *Phys. Rev. Lett.* **87** 215502

[4] Baughman R H, Zakhibov A A and de Heer W A 2002 Carbon nanotubes—the route toward applications *Science* **297** 787–92

[5] Cao Q and Rogers J A 2009 Ultrathin films of single-walled carbon nanotubes for electronics and sensors: a review of fundamental and applied aspects *Adv. Mater.* **21** 29–53

[6] Biercuk M J, Ilani S, Marcus C M and McEuen P L 2008 Electrical transport in single-wall carbon nanotubes *Carbon Nanotubes* (*Advanced Topics in the Synthesis, Structure, Properties and Applications*) ed A Jorio, G Dresselhaus and M S Dresselhaus (Berlin: Springer)

[7] Graham A P *et al* 2005 How do carbon nanotubes fit into the semiconductor roadmap? *Appl. Phys.* A **80** 1141–51

[8] Purewal M S, Hong B H, Ravi A, Chandra B, Hone J and Kim P 2007 Scaling of resistance and electron mean free path of single-walled carbon nanotubes *Phys. Rev. Lett.* **98** 186808

[9] Mann D, Javey A, Kong J, Wang Q and Dai H 2003 Ballistic transport in metallic nanotubes with reliable Pd ohmic contacts *Nano Lett.* **3** 1541–4

[10] Wei B Q, Vajtai R and Ajayan P M 2001 Reliability and current carrying capacity of carbon nanotubes *Appl. Phys. Lett.* **79** 1172–5

[11] Cassell A M and Li J 2007 Carbon nanotube based interconnect technology: opportunities and challenges *Micro- and Opto-Electronic Materials and Structures: Physics, Mechanics, Design, Reliability, Packaging* ed E Suhir, C P Wong and Y C Lee (New York: Springer)

[12] International technology roadmap for semiconductors 2009 Semiconductor Industry Association, San Jose, CA http://public.itrs.net

[13] Ting J-H, Chiu C-C and Huang F-Y 2009 Carbon nanotube array vias for interconnect applications *J. Vac. Sci. Technol.* B **27** 1086–92

[14] Coiffic J C, Fayolle M, Maitrejean S, Foa Torres L E F and Ponche H L 2007 Conduction regime in innovative carbon nanotube via interconnect *Appl. Phys. Lett.* **91** 252107

[15] Kreupl F, Graham A P, Liebau M, Duesber G S, Seidel R and Unger E 2004 Carbon nanotubes for interconnect applications *IEEE Int. Electron Devices Mtg* pp 683–6

[16] Park C, Ounaies Z, Watson K A, Crooks R E, Smith J Jr, Lowther S E, Connell J W, Siochi E J, Harrison J S and Clair T L St 2002 Dispersion of single wall carbon nanotubes by *in situ* polymerization under sonication. *Chem. Phys. Lett.* **364** 303–8

[17] Wu Z *et al* 2004 Transparent, conductive carbon nanotube films *Science* **305** 1273–6

[18] Shiraishi M and Ata M 2002 Conduction mechanisms in single-walled carbon nanotubes *Synth. Mat.* **128** 235–9

[19] Falvo M R, Clary G J, Taylor R M II, Chi V, Brooks F P Jr, Washburn S and Superfine R 1997 Bending and buckling of carbon nanotubes under large strain *Nature* **389** 582–4

[20] Kang S J, Kocabas C, Ozel T, Shim M, Pimparkar N, Alam M A, Rotkin S V and Rogers J A 2007 High-performance electronics using dense, perfectly aligned arrays of single-walled carbon nanotubes *Nat. Nanotechnol.* **2** 230–6

[21] LeMieux M C, Sok S, Roberts M E, Opatkiewicz J P, Liu D, Barman S N, Patil N, Mitra S and Bao Z 2009 Solution assembly of organized carbon nanotube networks for thin-film transistors *ACS Nano* **3** 4089–97

[22] Ishikawa F N, Chang H-K, Ryu K, Chen P-C, Badmaev A, Gomez De Arco L, Shen G and Zhou C 2009 Transparent electronics based on transfer printed aligned carbon nanotubes on rigid and flexible substrates *ACS Nano* **3** 73–9

[23] Engel M, Small J P, Steiner M, Freitag M, Green A A, Hersam M C and Avouris P 2008 Thin film nanotube transistors based on self-assembled, aligned semiconducting carbon nanotube arrays *ACS Nano* **2** 2445–52

[24] Novak J P, Snow E S, Houser E J, Park D, Stepnowski J L and McGill R A 2003 Nerve agent detection using networks of single-walled carbon nanotubes *Appl. Phys. Lett.* **83** 4026–8

[25] Snow E S, Perkins F K, Houser E J, Badescu S C and Reinecke T L 2005 Chemical detection with a single-walled carbon nanotube capacitor *Science* **307** 1942–5

[26] Bekyarova E, Davis M, Burch T, Itkis M E, Zhao B, Sunshine S and Haddon R C 2004 Chemically functionalized single-walled carbon nanotubes as ammonia sensors *J. Phys. Chem.* B **108** 19717–20

[27] Bondavalli P, Legagneux P and Pribat D 2009 Carbon nanotubes based transistors as gas sensors: state of the art and critical review *Sensors Actuators* B **140** 304–18

[28] Gruner G 2006 Carbon nanotube films for transparent and plastic electronics *J. Mater. Chem.* **16** 3533–9

[29] Pasquier A D, Unalan H E, Kanwal A, Miller S and Chhowalla M 2005 Conducting and transparent single-wall carbon nanotube electrodes for polymer-fullerene solar cells *Appl. Phys. Lett.* **87** 203511

[30] Barnes T M, Wu X, Zhou J, Duda A, van de Lagemaat J, Coutts T J, Weeks C L, Britz D A and Glatkowski P 2007 Single-wall carbon nanotube networks as a transparent back contact in CdTe solar cells *Appl. Phys. Lett.* **90** 243503

[31] Ago H, Petritsch K, Shaffer M S P, Windle A H and Friend R H 1999 Composites of carbon nanotubes and conjugated polymers for photovoltaics devices *Adv. Mater.* **11** 1281–5

[32] Contreras M A, Barnes T, van de Lagemaat J, Rumbles G, Coutts T J, Weeks C, Glatkowski P, Levitsky I, Peltola J and Britz D A 2007 Replacement of transparent conductive oxides by single-wall carbon nanotubes in Cu(In, Ga)De_2-based solar cells *J. Phys. Chem. Lett.* C **111** 14045–8

[33] Tenent R C, Barnes T M, Bergeson J D, Ferguson A J, To B, Gedvilas L M, Heben M J and Blackburn J L 2009 Ultrasmooth, large-area, high-uniformity, conductive transparent single-walled-carbon-nanotube films for photovoltaics produced by ultrasonic spraying *Adv. Mater.* **21** 3210–6

[34] Bachtold A, Henny M, Terrier C, Strunk C, Schönenberger C, Salvetat J-P, Bonard J-M and Forró L 1998 Contacting carbon nanotubes selectively with low ohmic-contacts for four-probe electric measurements *Appl. Phys. Lett.* **73** 274–6

[35] Liu Z, Jiao L, Yao Y, Xian X and Zhang J 2010 Aligned, ultralong single-walled carbon nanotubes: from synthesis, sorting, to electronic devices *Adv. Mater.* **22** 2285–310

[36] Yuzvinsky T D, Mickelson W, Aloni S, Konsek S L, Fennimore A M, Begtrup G E, Kis A, Regan B C and Zettl A 2005 Imaging the life story of nanotube devices *Appl. Phys. Lett.* **87** 083103

[37] Huang J Y, Chen S, Jo S H, Wang Z, Han D X, Chen G, Dresselhaus M S and Ren Z F 2005 Atomic-scale imaging of wall-by-wall breakdown and concurrent transport measurements in multiwall carbon nanotubes *Phys. Rev. Lett.* **94** 236802

[38] Collins P G, Hersam M, Arnold M, Martel R and Avouris Ph 2001 Current saturation and electrical breakdown in multiwalled carbon nanotubes *Phys. Rev. Lett.* **86** 3128–31

[39] Mølhave K, Gudnason S B, Pedersen A T, Clausen C H, Horsewell A and Bøgglid P 2006 Transmission electron microscopy study of individual carbon nanotube breakdown caused by Joule heating in air *Nano Lett.* **6** 1663–8

[40] Chung J, Lee K-H, Lee J, Troya D and Schatz G C 2004 Multi-walled carbon nanotubes experiencing electrical breakdown as gas sensors *Nanotechnology* **15** 1596–602

[41] Tsutsui M, Taninouchi Y-K, Kurokowa S and Sakai A 2006 Electrical breakdown of short multiwalled carbon nanotubes *J. Appl. Phys.* **100** 094302

[42] Pop E, Mann D A, Goodson K E and Dai H 2007 Electrical and thermal transport in metallic single-wall carbon nanotubes on insulating substrates *J. Appl. Phys.* **101** 093710

[43] Lan C, Amama P B, Fisher T S and Reifenberger R G 2007 Correlating electrical resistance to growth conditions for multiwalled carbon nanotubes *Appl. Phys. Lett.* **91** 093105

[44] Chai Y, Chan P C H, Fu Y, Chuang Y C and Liu C Y 2008 Electromigration studies of Cu/carbon nanotube composite interconnect using Blech structure *IEEE Electron Device Lett.* **29** 1001–3

[45] Chai Y, Zhang M, Gong J and Chan P C H 2006 Reliability evaluation of carbon nanotube interconnect in a silicon CMOS environment *Int. Conf. on Electronic Materials and Packaging (China)* pp 467–71

[46] Jaber-Ansari L, Hahm M G, Somu S, Sanz Y E, Busnaina A and Jung Y J 2009 Mechanism of very large scale assembly of SWNTs in template guided fluidic assembly process *J. Am. Chem. Soc.* **131** 804–8

[47] Xiong X, Jaberansari L, Hahm M G, Busnaina A and Jung Y J 2007 Building highly organized single-walled-carbon-nanotube networks using template guided fluidic assembly *Small* **3** 2006–10

[48] de Andrade M J, Lima M D, Skákalová V, Bergmann C P and Roth S 2007 Electrical properties of transparent carbon nanotube networks prepared through different techniques *Phys. Status Solidi* **1** 178–80

[49] Bekyarova E, Itkis M E, Cabrera N, Zhao B, Yu A, Gao J and Haddon R C 2005 Electronic properties of single-walled carbon nanotube networks *J. Am. Chem. Soc.* **127** 5990–5

[50] Blackburn J L, Barnes T M, Beard M C, Kim Y-H, Tenent R C, McDonald T J, To B, Coutts T J and Heben M J 2008 Transparent conductive single-walled carbon nanotube networks with precisely tunable ratios of semiconducting and metallic nanotubes *ACS Nano* **2** 1266–74

[51] Barnes T M, Blackburn J L, van de Lagemaat J, Coutts T J and Heben M J 2008 Reversibility, dopant desorption, and tunneling in the temperature-dependent conductivity of type-separated, conductive carbon nanotube networks *ACS Nano* **2** 1968–76

[52] Kaiser A B, Düsberg G and Roth S 1998 Heterogeneous model for conduction in carbon nanotubes *Phys. Rev.* B **57** 1418–21

[53] Saito T, Ashihara H, Ishikawa K, Miyauchi M, Yamada Y and Nakano H 2004 A reliability study of barrier-metal-clad copper interconnects with self-aligned metallic caps *IEEE Trans. Electron Devices* **51** 2129–34

[54] Filippi R G, Wang P-C, Brendler A and Lloyd J R 2009 Correlation between a threshold failure time and void nucleation for describing the bimodal electromigration behavior of copper interconnects *Appl. Phys. Lett.* **95** 072111

[55] Tan C M, Roy A, Vairagar A V, Krishnamoorthy A and Mhaisalkar S G 2005 Current crowding effect on copper dual damascene via bottom failure for ULSI applications *IEEE Trans. Device Mater. Reliab.* **5** 198–205

[56] Scorzoni A, Munari I D and Stulens H 1994 Non-destructive electrical techniques as a means for understanding the basic mechanisms of electromigration *Mater. Res. Soc. Symp. Proc.* **337** 515–26

[57] Rosenberg R and Berenbaum L 1968 Resistance monitoring and effects of nanoadhesion during electromigration in aluminum films *Appl. Phys. Lett.* **12** 201–4

[58] Munari I D, Scorzoni A, Tamarri F and Fantini F 1995 Activation energy in the early stage of electromigration in Al-1% Si/TiN/Ti bamboo lines *Semicond. Sci. Technol.* **10** 255–9

[59] Wei F L, Gan C L, Tan T L, Hau-Riege C S, Marathe A P, Vlassak J J and Thompson C V 2008 Electromigration-induced extrusion failures in Cu/low-k interconnects *J. Appl. Phys.* **104** 023529

[60] Hu L, Hecht D S and Gruner G 2004 Percolation in transparent and conducting carbon nanotube networks *Nano Lett.* **4** 2513–7

[61] Topinka M A, Rowell M W, Goldhaber-Gordon D, McGehee M D, Hecht D S and Gruner G 2009 Charge transport in interpenetrating networks of semiconducting and metallic carbon nanotubes *Nano Lett.* **9** 1866–71

[62] Estrada D and Pop E 2011 Imaging dissipation and hot spots in carbon nanotube network transistors *Appl. Phys. Lett.* **98** 073102

[63] Nirmalraj P N, Lyons P E, De S, Coleman J N and Boland J J 2009 Electrical connectivity in single-walled carbon nanotube networks *Nano Lett.* **9** 3890–5

[64] Collins P G, Bradley K, Ishigami M and Zettl A 2000 Extreme oxygen sensitivity of electronic properties of carbon nanotubes *Science* **287** 1801–4

[65] Jackson R K, Munro A, Nebesny K, Armstrong N and Graham S 2010 Evaluation of transparent carbon nanotube networks of homogeneous electronic type *ACS Nano* **4** 1377–84

[66] Zahab A, Spina L, Poncharal P and Marliére C 2000 Charge transfer and fermi level shift in p-doped single-walled carbon nanotubes *Phys. Rev.* B **62** 10000–3
[67] Salehi-Khojin A, Lin K Y, Field C R and Masel R I 2010 Nonthermal current-stimulated desorption of gases from carbon nanotubes *Science* **329** 1327–30
[68] Williams E W, Lawlor C M, Keeling A G and Gould R D 1994 Novel room temperature carbon monoxide sensor utilizing rate of change of resistance in thick films of tin oxide *Int. J. Electron.* **76** 815–20
[69] Vijayaraghavan A, Marquardt C W, Dehm S, Hennrich F and Krupke R 2010 Imaging defects and junctions in single-walled carbon nanotubes by voltage-contrast scanning electron microscopy *Carbon* **48** 494–500
[70] Stadermann M *et al* 2004 Nanoscale study of conduction through carbon nanotube networks *Phys. Rev.* B **69** 201402(R)
[71] Kim Y L *et al* 2009 Highly aligned scalable platinum-decorated single-wall carbon nanotube arrays for nanoscale electrical interconnects *ACS Nano* **3** 2818–26